Nano Research 2017, 10(12): 4298–4304
DOI 10.1007/s12274-016-1394-1
Research Article
ISSN 1998-0124
CN 11-5974/O4

Embedding CoS_2 nanoparticles in N-doped carbon nanotube hollow frameworks for enhanced lithium storage properties

Jintao Zhang, Le Yu (✉), and Xiong Wen (David) Lou (✉)

School of Chemical and Biomedical Engineering, Nanyang Technological University, 62 Nanyang Drive, Singapore 637459, Singapore

Received: 15 September 2016
Revised: 22 November 2016
Accepted: 28 November 2016

KEYWORDS
CoS_2,
carbon nanotube,
metal-organic framework,
lithium-ion batteries

ABSTRACT

The construction of metal sulfides-carbon nanocomposites with a hollow structure is highly attractive for various energy storage and conversion technologies. Herein, we report a facile two-step method for preparing a nanocomposite with CoS_2 nanoparticles in N-doped carbon nanotube hollow frameworks (NCNTFs). Starting from zeolitic imidazolate framework-67 (ZIF-67) particles, *in situ* reduced metallic cobalt nanocrystals expedite the formation of the hierarchical hollow frameworks from staggered carbon nanotubes via a carbonization process. After a follow-up sulfidation reaction with sulfur powder, the embedded cobalt crystals are transformed into CoS_2 nanoparticles. Benefitting from the robust hollow frameworks made of N-doped carbon nanotubes and highly active CoS_2 ultrafine nanoparticles, this advanced nanocomposite shows greatly enhanced lithium storage properties when evaluated as an electrode for lithium-ion batteries. Impressively, the resultant CoS_2/NCNTF material delivers a high specific capacity of ~937 mAh·g^{-1} at a current density of 1.0 A·g^{-1} with a cycle life longer than 160 cycles.

1 Introduction

Lithium-ion batteries (LIBs) are promising electrical energy-storage devices for addressing the imminent shortage of fossil fuels and growing environmental concerns [1–3]. LIBs based on the traditional carbonaceous electrode materials are approaching their theoretical power/energy density limit [4, 5]. Therefore, the elaborate exploration and rational design of new electrode materials are crucial for realizing new generations of high-performance LIBs [6–8]. Among numerous candidates, metal sulfides have received growing attention as advanced anodes owing to their high theoretical capacity arising from their rich stoichiometric compositions and better electrical conductivity compared with their corresponding metal oxide counterparts [9–14]. However, their practical applications are hampered by pronounced volume expansion and contraction during the repetitive charging/discharging processes and sluggish ion/

Address correspondence to Xiong Wen (David) Lou, xwlou@ntu.edu.sg; Le Yu, yule0001@e.ntu.edu.sg

electron-transport kinetics, which result in a poor cycle life and unsatisfactory rate performance [15–17].

Hollow-structured micro/nanomaterials have proven their superiority as smart architectures for LIBs by providing extra space to alleviate the dramatic (de)lithiation strain and maintain the integrity of electrodes [18–22]. The utilization of hollow structures in combination with conductive carbon materials is promising for ameliorating the conductivity of metal sulfides and buffering volumetric changes during electrochemical reactions [23–27]. For example, Yu et al. reported the synthesis of a unique hybrid hollow structure by assembling ultrathin MoS_2 nanosheets on N-doped carbon shells, which exhibited a high capacity, long cycle life, and superior rate performance for LIBs [23]. Zou et al. prepared hollow polyhedral composites of porous carbon/short carbon nanotube-stabilized CoS nanoparticles through a one-step simultaneous pyrolysis and sulfidation treatment of zeolitic imidazolate framework-67 (ZIF-67) precursors [24]. Owing to the strong coupling effect of the unique hybrids, the novel hollow structures exhibited superior electrochemical properties as an anode material for LIBs. Notwithstanding these advances, many carbon materials in previously reported nanocomposites are microporous, with a poor graphitic degree, which is not beneficial for ion and electron transport. In comparison, a hierarchical hollow framework involving interconnected highly conductive carbon nanotube networks might be an ideal host for loading metal sulfides, not only offering abundant active sites and a porous structure for fast charge transport and mass transfer but also helping to buffer the volume expansion/contraction upon cycling [28].

Herein, we report a two-step metal-organic-framework-engaged method for preparing CoS_2 nanoparticles in hollow carbonaceous N-doped carbon nanotube frameworks (NCNTFs). The hierarchical NCNTFs are converted from the thermal decomposition of ZIF-67 crystals in the presence of hydrogen as a conductive matrix. Metallic cobalt nanoparticles are uniformly embedded within the three-dimensional carbon nanotube frameworks and transformed into CoS_2 ultrafine nanocrystals after a sulfidation reaction with sulfur powder at an elevated temperature. Encouragingly, the as-obtained novel CoS_2/NCNTF nanocomposite exhibits a remarkably enhanced lithium storage performance as an anode material for LIBs.

2 Experimental

2.1 Synthesis of ZIF-67 polyhedrons

All the chemicals were directly used as received. ZIF-67 polyhedrons were synthesized using a method that we previously reported [29]. In a typical procedure, 1 mmol of $Co(NO_3)_2{\cdot}6H_2O$ and 4 mmol of 2-methylimidazole were dissolved in 25 mL of methanol. Then, the solution of 2-methylimidazole was quickly poured into a solution of $Co(NO_3)_2$ under vigorous stirring. The mixed solution was aged for one day at the ambient temperature. Finally, the purple precipitate was washed with ethanol three times by centrifugation and dried for future use.

2.2 Synthesis of Co/NCNTFs

The ZIF-67 particles were heated to 350 °C and maintained for 1.5 h under an Ar/H_2 flow (95%/5% in volume ratio). Then, the temperature was further increased to 700 °C and maintained for 3.5 h. The ramp rate was fixed at 2 °C·min^{-1} for these two processes.

2.3 Synthesis of CoS_2/NCNTFs

The obtained Co/NCNTF materials were mixed with sulfur powder at a mass ratio of 1:2. Then, the mixture was heated to 300 °C at a ramp rate of 10 °C·min^{-1} and maintained for 2 h in a tube furnace under a N_2 flow. Finally, the furnace was cooled to room temperature naturally.

2.4 Materials characterization

The morphologies and structures were characterized by field-emission scanning electron microscopy (FESEM; JEOL, JEM-6701F, 5 kV) and transmission electron microscopy (TEM; JEOL, JEM-2010, 200 kV). Powder X-ray diffraction (XRD) patterns were recorded using a Bruker diffractometer with Cu Kα radiation (D2 phaser, Cu Kα, λ = 1.5406 Å) to examine the crystallographic structure. The composition of the samples was analyzed using an energy-dispersive X-ray spectroscope attached to the FESEM instrument. The

N_2 sorption isotherms were examined at the liquid-nitrogen temperature. The Raman spectra of the dried samples were collected using a Renishaw System 1000 micro-Raman spectroscope. Thermogravimetric analysis (TGA, Perkin Pyris Diamond) was performed under an air flow (200 mL·min^{-1}) with a ramp rate of 10 °C·min^{-1}.

2.5 Electrochemical measurements

The working electrode was composed of the active material, carbon black (Ketjenblack), and a polymer binder (polyvinylidene fluoride) at a weight ratio of 70:20:10. This mixture was pressed onto Cu foil and dried at 70 °C for 24 h. The mass loading of electroactive materials was ~1.0 mg·cm^{-2}. Pure lithium foil was used as both the counter electrode and the reference electrode. The electrolyte was composed of $LiPF_6$ (1.0 M) in a 50:50 (w/w) mixture of ethylene carbonate and diethyl carbonate. Cell assembly was performed in an Ar-filled glovebox with concentrations of moisture and oxygen below 1.0 ppm. Galvanostatic charge/discharge tests were performed using a NEWARE battery tester with a cut-off voltage window of 0.05–3.0 V versus Li/Li$^+$.

3 Results and discussion

Figure 1 schematically illustrates the synthesis of the hierarchical CoS_2/NCNTFs. Well-defined ZIF-67 polyhedrons prepared via a precipitation method are selected as the starting material. Next, a facile thermal treatment in the Ar/H_2 atmosphere transforms the solid ZIF-67 particle into a hybrid structure of Co/NCNTFs. During the heating process in the strongly reducing gas, *in situ* generated elemental Co nanoparticles are highly active, catalyzing the growth of CNTs using carbon sources derived from organic ligands in ZIF-67 [30–32]. After a follow-up sulfidation reaction with sulfur, the confined Co particles are converted into ultrafine CoS_2 nanocrystals embedded within the hierarchical carbon nanotube framework.

After the annealing treatment in Ar/H_2, the morphology and microstructure of the Co/NCNTF products are examined by FESEM. As shown in Fig. 2(a), the as-obtained composite particles are quite uniform with a rhombic dodecahedron shape, which is inherited

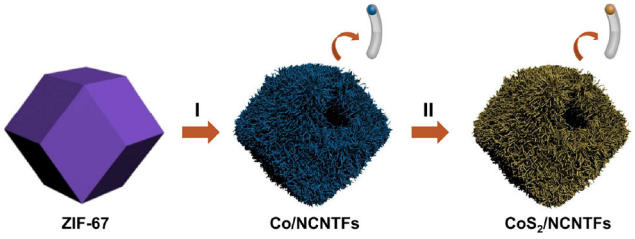

Figure 1 Schematic of the formation process of CoS_2/NCNTFs.

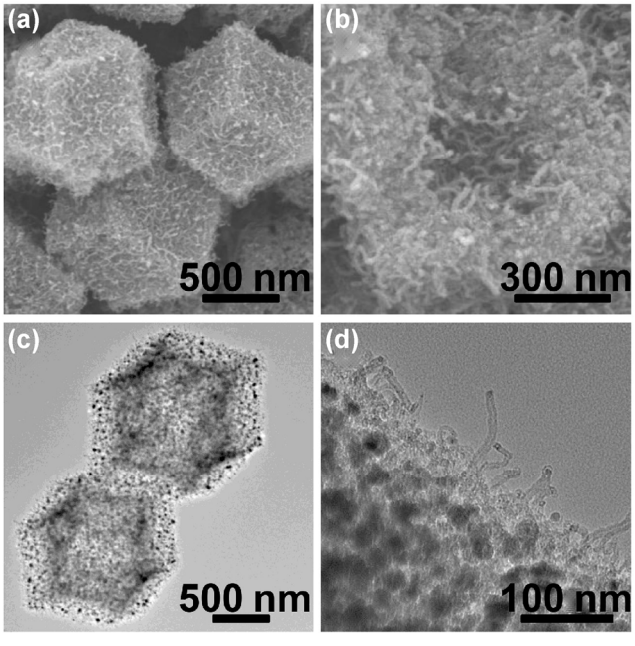

Figure 2 FESEM images of (a) Co/NCNTFs and (b) a broken particle. TEM images of (a) Co/NCNTFs and (d) the hierarchical shell.

from the ZIF-67 precursor (Fig. S1 in the Electronic Supplementary Material (ESM)). In contrast to its solid precursor with a smooth surface, the Co/NCNTF hybrid is rough on surface, which is entwined by numerous interlaced CNTs. Moreover, the internal void space of the framework with a shell thickness of ~300 nm is clearly revealed by the broken Co/NCNTF particle shown in Fig. 2(b). The hollow interior and detailed geometrical structure of the as-synthesized hierarchical structures are further elucidated by TEM observation in Fig. 2(c). Figure 2(d) shows a partially enlarged view of the composite shell, confirming the existence of Co nanoparticles embedded at the tips of CNTs. The corresponding XRD pattern (Fig. S2(a) in the ESM) corroborates the complete transformation from ZIF-67 to Co/NCNTFs. Compared with metallic Co, which has distinct diffraction peaks, the signals of

the carbon nanotubes are relatively weak. The energy-dispersive X-ray spectroscopy (EDX) spectrum (Fig. S2(b) in the ESM) confirms the large amount of Co in the nanocomposite. Additionally, the EDX results indicate the existence of nitrogen species, which are beneficial for modifying the chemical and electronic properties of the carbon host [13, 23, 27]. The Raman spectrum of the Co/NCNTF product provides information about the characteristic G and D bands of the carbon material (Fig. S3 in the ESM), which are related to the sp^2-carbon and disordered or defect carbon due to the microstructure rearrangement and the incorporation of N atoms during the transformation [31, 33]. As indicated by the Raman spectrum, the peak intensity of the G band is slightly higher than that of the D band, indicating a relatively high graphenic order.

After the sulfidation reaction with sulfur, the Co particles within the Co/NCNTF composite are successfully converted into CoS_2. All the visible Bragg peaks in the XRD spectrum (Fig. S4(a) in the ESM) for the final product are perfectly indexed to CoS_2 (JCPDS card No.: 03-0772). The EDX spectrum confirms the existence of a large amount of sulfur species with a Co/S atomic ratio of ~0.49 (Fig. S4(b) in the ESM). The FESEM image in Fig. 3(a) elucidates the well-retained overall polyhedral morphology of the materials, indicating their robust structural stability. A magnified view of an individual particle (Fig. 3(b)) demonstrates that the exterior CNTs can survive repetitive annealing without apparent agglomeration. TEM examinations (Figs. 3(c) and 3(d)) confirm that the sulfurized samples retain the structural features of the Co/NCNTFs well. Moreover, highly uniform hollow structures are observed, and the inner cavities are unambiguously revealed by the sharp contrast between the hierarchical CoS_2/NCNTF shell and the hollow interior. A closer TEM view (Fig. 3(e)) shows that these CNTs have a length of several hundred nanometers with an ultrafine CoS_2 particle enclosed at the tip. Consistent with the XRD analysis, the high-resolution TEM (HRTEM) image in Fig. 3(f) verifies that these CoS_2 crystals are crystalline with an inter-planar distance of ~0.27 nm corresponding to the (200) plane of CoS_2. TGA is employed to determine the amount of CoS_2 in the CoS_2/NCNTF product. According to the TGA data (Fig. S5 in the ESM), the CoS_2 content in the sample is estimated to be 46 wt.% [31]. Owing to its hollow structure and highly porous shell, the hierarchical CoS_2/NCNTF composite sample exhibits a large specific Brunauer–Emmett–Teller surface area of 110.4 $m^2 \cdot g^{-1}$ (Fig. S6 in the ESM). The pore-size distribution curve indicates that the majority of these pores range from 2 to 10 nm in size.

Next, we perform an electrochemical evaluation

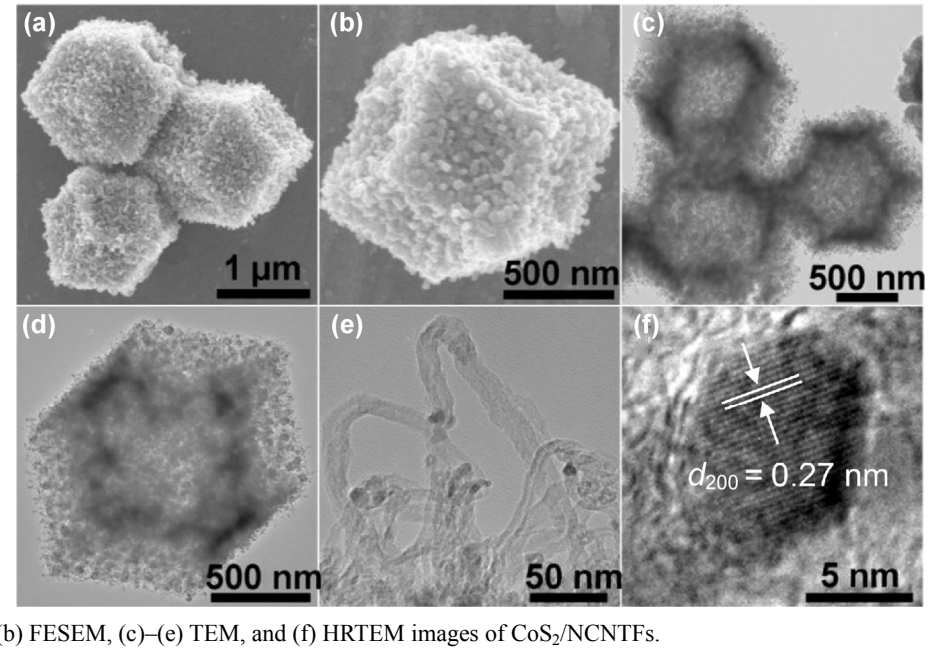

Figure 3 (a) and (b) FESEM, (c)–(e) TEM, and (f) HRTEM images of CoS_2/NCNTFs.

of the CoS_2/NCNTFs as an anode material for LIBs. Figure 4(a) presents the charge–discharge voltage profiles for the first two cycles at a constant current density of 1.0 $A \cdot g^{-1}$. The first discharge and charge specific capacities are approximately 1,187 and 927 $mAh \cdot g^{-1}$, respectively, leading to an initial Coulombic efficiency (CE) of ~78%. The irreversible capacity could be due to the formation of the solid–electrolyte interface film and the decomposition of the electrolyte, which is a common drawback of nanostructured anodes. In the first discharge curve, three discernable plateaus are observed. The voltage plateaus in the ranges of 1.8–1.6 and 1.5–1.2 V are related to the insertion of a small amount of Li^+ ions and the displacement reaction of Li_2S and Co, respectively [13, 22]. During the second cycle, small voltage shifts for these two peaks towards higher potentials are observed, which are mainly attributed to the structural variation of the electrode materials. The representative cyclic-voltammetry (Fig. S7 in the ESM) curves of the composite electrode agree well with the plateaus of the galvanostatic-discharge curves, confirming the multi-step electrochemical processes of the CoS_2-based electrode. Figure 4(b) shows the cycling stability of the CoS_2/NCNTF electrode tested by galvanostatic measurements at different current rates. The reversible discharge capacities of the as-prepared electrode are approximately 1,191, 952, 779, and 615 $mAh \cdot g^{-1}$ at current densities of 0.2, 0.5, 1.0, and 2.0 $A \cdot g^{-1}$, respectively. Even at a relatively high current density of 5.0 $A \cdot g^{-1}$, the electrode delivers a specific capacity as high as 439 $mAh \cdot g^{-1}$, demonstrating its excellent high-rate capability. Importantly, the capacity recovers to 1,040 $mAh \cdot g^{-1}$ when the current density returns to 0.2 $A \cdot g^{-1}$. Notably, the CoS_2/NCNTF electrode also exhibits remarkable cycling stability at a constant charge–discharge current density of 1.0 $A \cdot g^{-1}$. As shown in Fig. 4(c), the discharge capacity is quickly stabilized from the second cycle onwards and maintained at a high value of ~937 $mAh \cdot g^{-1}$ after 160 cycles. The CE for the CoS_2/NCNTF composite electrode is close to 100% after the first cycle. Overall, this performance is superior or comparable to that of many other cobalt sulfides-based anodes (Table S1 in the ESM) [13, 18, 22, 24, 34–36]. The remarkable performance of CoS_2/NCNTFs is attributed to their unique structural and compositional features. Specifically, the construction of ultrafine CoS_2 nanoparticles embedded in the carbon

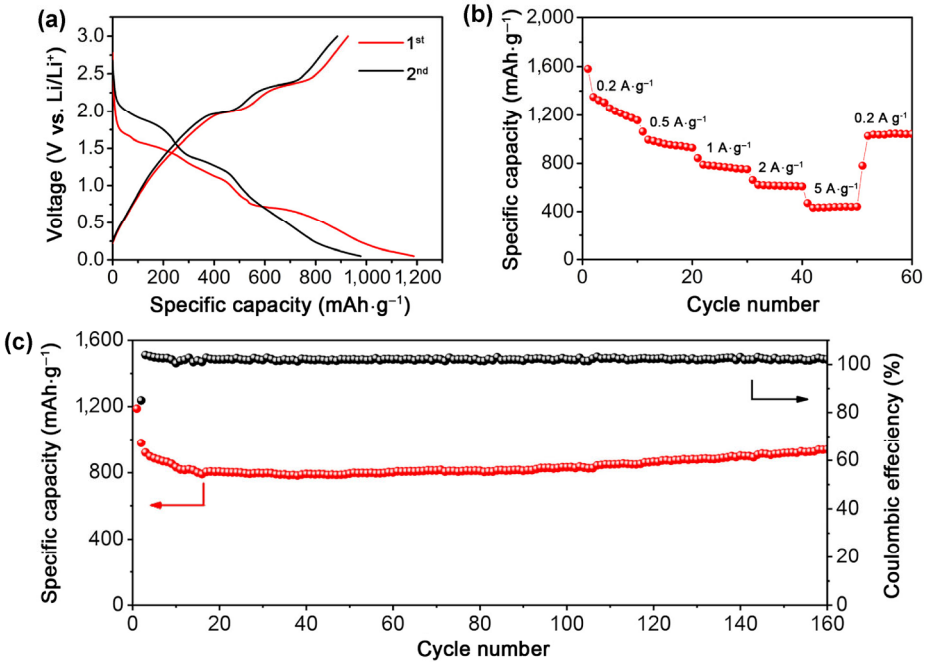

Figure 4 Electrochemical evaluation of the CoS_2/NCNTF electrode. (a) Galvanostatic charge–discharge voltage profiles at 1.0 $A \cdot g^{-1}$. (b) Rate-capability test at various current densities; (c) cycling performance at 1.0 $A \cdot g^{-1}$ and the corresponding CE. All measurements are conducted in the voltage range of 0.05–3.0 V versus Li/Li^+.

frameworks not only enables a short diffusion distance for the fast diffusion of Li^+ ions but also provides sufficient contact between the active material and the electrolyte for the rapid charge-transfer reaction. Additionally, the hollow architectures composed of interconnected CNTs provide sufficient space for effectively withstanding large volume variations upon cycling, resulting in good structural integrity.

4 Conclusions

We report the rational design and synthesis of CoS_2 nanoparticles embedded in NCNTFs via the direct pyrolysis of metal-organic frameworks and a subsequent sulfidation treatment. The resultant interconnected carbonaceous frameworks provide high conductivity and structural stability for well-dispersed CoS_2 ultrafine nanoparticles. Owing to their prominent structural and compositional advantages, the as-prepared hierarchically structured CoS_2-carbon nanocomposite manifests enhanced lithium storage properties with high specific capacities at various current densities and an excellent cycling stability as an anode material for lithium-ion batteries.

Electronic Supplementary Material: Supplementary material (FESEM images, TEM images, XRD patterns, TGA curve, Raman spectroscopy measurement, N_2 adsorption–desorption isotherms, and additional electrochemical measurements) is available in the online version of this article at http://dx.doi.org/10.1007/s12274-016-1394-1

References

[1] Goodenough, J. B. Evolution of strategies for modern rechargeable batteries. *Acc. Chem. Res.* **2013**, *46*, 1053–1061.

[2] Simon, P.; Gogotsi, Y.; Dunn, B. Where do batteries end and supercapacitors begin? *Science* **2014**, *343*, 1210–1211.

[3] Yuan, C. Z.; Wu, H. B.; Xie, Y.; Lou, X. W. Mixed transition-metal oxides: Design, synthesis, and energy-related applications. *Angew. Chem., Int. Ed.* **2014**, *53*, 1488–1504.

[4] Reddy, M. V.; Rao, G. V. S.; Chowdari, B. V. R. Metal oxides and oxysalts as anode materials for Li ion batteries. *Chem. Rev.* **2013**, *113*, 5364–5457.

[5] Xin, S.; Guo, Y. G.; Wan, L. J. Nanocarbon networks for advanced rechargeable lithium batteries. *Acc. Chem. Res.* **2012**, *45*, 1759–1769.

[6] Jiang, J.; Li, Y. Y.; Liu, J. P.; Huang, X. T.; Yuan, C. Z.; Lou, X. W. Recent advances in metal oxide-based electrode architecture design for electrochemical energy storage. *Adv. Mater.* **2012**, *24*, 5166–5180.

[7] Liu, C.; Li, F.; Ma, L. P.; Cheng, H. M. Advanced materials for energy storage. *Adv. Mater.* **2010**, *22*, E28–E62.

[8] Ji, L. W.; Lin, Z.; Alcoutlabi, M.; Zhang, X. W. Recent developments in nanostructured anode materials for rechargeable lithium-ion batteries. *Energy Environ. Sci.* **2011**, *4*, 2682–2699.

[9] Huang, X.; Zeng, Z. Y.; Zhang, H. Metal dichalcogenide nanosheets: Preparation, properties and applications. *Chem. Soc. Rev.* **2013**, *42*, 1934–1946.

[10] Yu, X. Y.; Yu, L.; Lou, X. W. Metal sulfide hollow nanostructures for electrochemical energy storage. *Adv. Energy Mater.* **2016**, *6*, 1501333

[11] Shen, L. F.; Yu, L.; Wu, H. B.; Yu, X. Y.; Zhang, X. G.; Lou, X. W. Formation of nickel cobalt sulfide ball-in-ball hollow spheres with enhanced electrochemical pseudocapacitive properties. *Nat. Commun.* **2015**, *6*, 6694.

[12] Yu, L.; Zhang, L.; Wu, H. B.; Lou, X. W. Formation of $Ni_xCo_{3-x}S_4$ hollow nanoprisms with enhanced pseudocapacitive properties. *Angew. Chem., Int. Ed.* **2014**, *53*, 3711–3714.

[13] Wang, Q. F.; Zou, R. Q.; Xia, W.; Ma, J.; Qiu, B.; Mahmood, A.; Zhao, R.; Yang, Y. Y. C.; Xia, D. G.; Xu, Q. Facile synthesis of ultrasmall CoS_2 nanoparticles within thin N-doped porous carbon shell for high performance lithium-ion batteries. *Small* **2015**, *11*, 2511–2517.

[14] Xu, X. D.; Liu, W.; Kim, Y.; Cho, J. Nanostructured transition metal sulfides for lithium ion batteries: Progress and challenges. *Nano Today* **2014**, *9*, 604–630.

[15] Rui, X. H.; Tan, H. T.; Yan, Q. Y. Nanostructured metal sulfides for energy storage. *Nanoscale* **2014**, *6*, 9889–9924.

[16] Su, Q. M.; Xie, J.; Zhang, J.; Zhong, Y. J.; Du, G. H.; Xu, B. S. *In situ* transmission electron microscopy observation of electrochemical behavior of CoS_2 in lithium-ion battery. *ACS Appl. Mater. Interfaces* **2014**, *6*, 3016–3022.

[17] Wang, J.; Liu, J. L.; Chao, D. L.; Yan, J. X.; Lin, J. Y.; Shen, Z. X. Self-assembly of honeycomb-like MoS_2 nanoarchitectures anchored into graphene foam for enhanced lithium-ion storage. *Adv. Mater.* **2014**, *26*, 7162–7169.

[18] Yu, L.; Yang, J. F.; Lou, X. W. Formation of CoS_2 nanobubble hollow prisms for highly reversible lithium storage. *Angew. Chem., Int. Ed.* **2016**, *55*, 13422–13426.

[19] Wang, P. P.; Sun, H. Y.; Ji, Y. J.; Li, W. H.; Wang, X. Three-dimensional assembly of single-layered MoS_2. *Adv. Mater.* **2014**, *26*, 964–969.

[20] Zhou, Y. L.; Yan, D.; Xu, H. Y.; Feng, J. K.; Jiang, X. L.; Yue, J.; Yang, J.; Qian, Y. T. Hollow nanospheres of

mesoporous Co_9S_8 as a high-capacity and long-life anode for advanced lithium ion batteries. *Nano Energy* **2015**, *12*, 528–537.

[21] Ko, Y. N.; Choi, S. H.; Park, S. B.; Kang, Y. C. Preparation of yolk–shell and filled Co_9S_8 microspheres and comparison of their electrochemical properties. *Chem.—Asian J.* **2014**, *9*, 572–576.

[22] Wang, Q. H.; Jiao, L. F.; Han, Y.; Du, H. M.; Peng, W. X.; Huan, Q. N.; Song, D. W.; Si, Y. C.; Wang, Y. J.; Yuan, H. T. CoS_2 hollow spheres: Fabrication and their application in lithium-ion batteries. *J. Phys. Chem. C* **2011**, *115*, 8300–8304.

[23] Yu, X. Y.; Hu, H.; Wang, Y. W.; Chen, H. Y.; Lou, X. W. Ultrathin MoS_2 nanosheets supported on N-doped carbon nanoboxes with enhanced lithium storage and electrocatalytic properties. *Angew. Chem., Int. Ed.* **2015**, *54*, 7395–7398.

[24] Wu, R. B.; Wang, D. P.; Rui, X. H.; Liu, B.; Zhou, K.; Law, A. W. K.; Yan, Q. Y.; Wei, J.; Chen, Z. *In-situ* formation of hollow hybrids composed of cobalt sulfides embedded within porous carbon polyhedra/carbon nanotubes for high-performance lithium-ion batteries. *Adv. Mater.* **2015**, *27*, 3038–3044.

[25] Liu, J.; Wu, C.; Xiao, D. D.; Kopold, P.; Gu, L.; van Aken, P. A.; Maier, J.; Yu, Y. MOF-derived hollow Co_9S_8 nanoparticles embedded in graphitic carbon nanocages with superior Li-ion storage. *Small* **2016**, *12*, 2354–2364.

[26] Meng, X. B.; He, K.; Su, D.; Zhang, X. F.; Sun, C. J.; Ren, Y.; Wang, H. H.; Weng, W.; Trahey, L.; Canlas, C. P. et al. Gallium sulfide-single-walled carbon nanotube composites: High-performance anodes for lithium-ion batteries. *Adv. Funct. Mater.* **2014**, *24*, 5435–5442.

[27] Peng, S. J.; Li, L. L.; Mhaisalkar, S. G.; Srinivasan, M.; Ramakrishna, S.; Yan, Q. Y. Hollow nanospheres constructed by CoS_2 nanosheets with a nitrogen-doped-carbon coating for energy-storage and photocatalysis. *ChemSusChem* **2014**, *7*, 2212–2220.

[28] Huang, G.; Zhang, F. F.; Du, X. C.; Qin, Y. L.; Yin, D. M.; Wang, L. M. Metal organic frameworks route to *in situ* insertion of multiwalled carbon nanotubes in Co_3O_4 polyhedra as anode materials for lithium-ion batteries. *ACS Nano* **2015**, *9*, 1592–1599.

[29] Zhang, J. T.; Hu, H.; Li, Z.; Lou, X. W. Double-shelled nanocages with cobalt hydroxide inner shell and layered double hydroxides outer shell as high-efficiency polysulfide mediator for lithium–sulfur batteries. *Angew. Chem., Int. Ed.* **2016**, *55*, 3982–3986.

[30] Chen, Y. M.; Li, X. Y.; Park, K.; Song, J.; Hong, J. H.; Zhou, L. M.; Mai, Y. W.; Huang, H. T.; Goodenough, J. B. Hollow carbon-nanotube/carbon-nanofiber hybrid anodes for Li-ion batteries. *J. Am. Chem. Soc.* **2013**, *135*, 16280–16283.

[31] Xia, B. Y.; Yan, Y.; Li, N.; Wu, H. B.; Lou, X. W.; Wang, X. A metal–organic framework-derived bifunctional oxygen electrocatalyst. *Nat. Energy* **2016**, *1*, 15006.

[32] Huang, X. K.; Cui, S. M.; Chang, J. B.; Hallac, P. B.; Fell, C. R.; Luo, Y. T.; Metz, B.; Jiang, J. W.; Hurley, P. T.; Chen, J. H. A hierarchical tin/carbon composite as an anode for lithium-ion batteries with a long cycle life. *Angew. Chem., Int. Ed.* **2015**, *54*, 1490–1493.

[33] Ferrari, A. C. Raman spectroscopy of graphene and graphite: Disorder, electron-phonon coupling, doping and nonadiabatic effects. *Solid State Commun.* **2007**, *143*, 47–57.

[34] Jin, R. C.; Zhou, J. H.; Guan, Y. S.; Liu, H.; Chen, G. Mesocrystal Co_9S_8 hollow sphere anodes for high performance lithium ion batteries. *J. Mater. Chem. A* **2014**, *2*, 13241–13244.

[35] Qiu, W. D.; Jiao, J. Q.; Xia, J.; Zhong, H. M.; Chen, L. P. A self-standing and flexible electrode of yolk-shell CoS_2 spheres encapsulated with nitrogen-doped graphene for high-performance lithium-ion batteries. *Chem.—Eur. J.* **2015**, *21*, 4359–4367.

[36] Jin, R. C.; Yang, L. X.; Li, G. H.; Chen, G. Hierarchical worm-like CoS_2 composed of ultrathin nanosheets as an anode material for lithium-ion batteries. *J. Mater. Chem. A* **2015**, *3*, 10677–10680.